

Depinning of Multiphase Fluid Using Light and Photo-Responsive Surfactants

Lei Zhao^{1§}, Serena Seshadri^{2§}, Xichen Liang³, Sophia J. Bailey², Michael Haggmark³, Michael Gordon³, Matthew E. Helgeson³, Javier Read de Alaniz^{2*} (email: jalaniz@ucsb.edu), Paolo Luzzatto-Fegiz^{1*} (email: pfegez@ucsb.edu), Yangying Zhu^{1*} (email: yangying@ucsb.edu)

¹Department of Mechanical Engineering, University of California, Santa Barbara, Santa Barbara, California 93106-5070, USA

²Department of Chemistry, University of California at Santa Barbara, Santa Barbara, California 93106-5070, USA

³Department of Chemical Engineering, University of California at Santa Barbara, Santa Barbara, California 93106-5070, USA

§These authors contributed equally to this work

* To whom correspondence should be addressed

ABSTRACT

The development of non-invasive and robust strategies for manipulation of droplets and bubbles is crucial in applications such as boiling and condensation, electrocatalysis and microfluidics. In this work, we realize the swift departure of droplets and bubbles from solid substrates by introducing photo-responsive surfactants and applying asymmetric illumination, thereby inducing a “photo-Marangoni” lift force. Experiments show that a pinned toluene droplet can depart the substrate in only 0.38 s upon illumination, and that the volume of an air bubble at departure is reduced by 20%, indicating significantly faster departure. These benefits can be achieved with moderate light intensities and dilute surfactant concentrations, without specially fabricated substrates, which greatly facilitates practical applications. Simulations suggest that the net departure force includes contributions from viscous stresses directly caused by the Marangoni flow, as well as from pressure buildup due to flow stagnation at the contact line. The manipulation scheme proposed here shows potential for applications requiring droplet and bubble removal from working surfaces.

Introduction

Dynamic control of fluid motion in a multi-phase system offers exciting and transformative manipulation capabilities for a wide spectrum of laboratory and industrial applications, such as phase-change heat transfer¹, water harvesting², electro-catalysis³. For example, the critical heat flux (CHF) in boiling heat transfer, which is the maximum heat flux before the nucleate boiling regime breaks down, can be enhanced by over 100% by surfaces that facilitate bubble formation and departure^{4,5}. Similarly, the fabrication and manufacturing of multi-scale and multi-phase materials⁶ necessitates the precise and rapid control of precursors, such as prescribing the alignment of fibers, to achieve desired material properties with high throughput⁷. Past research efforts explored the use of coatings and surface structures to passively control fluid behaviors⁸⁻¹¹, whereas recent advances have enabled dynamic manipulation of bubble and droplet motions by introducing materials that respond to thermal¹², chemical¹³, electrical¹⁴, or magnetic stimuli¹⁵. Notably, electrowetting-on-dielectrics systems can precisely move, merge, and split discrete droplets¹⁶. However, thermally and chemically actuated systems typically have long response times and reversibility issues. Electrowetting and magnetically controlled systems generally require high voltages¹⁷ or strong magnetic fields¹⁸, with implications for reliability and safety. In addition, sophisticatedly patterned electrodes are needed, complicating practical implementations.

Recently, stimuli-responsive surfactants have emerged as an attractive alternative for dynamic manipulation. Recent work has utilized ionic surfactants to dynamically change the friction coefficient¹⁹, wettability²⁰ and the onset of nucleate boiling²¹, by controlling the attraction to a surface using an electric field requiring only a few Volt. However, to realize spatial control, such an approach still requires pre-patterned electrodes, which limits spatial resolution and real-time reconfigurability. An alternative approach leverages photo-responsive surfactants, which can reversibly switch molecular conformation and thereby change interfacial tension when illuminated at specific wavelengths (Figure 1a). They are exciting candidates for dynamic fluid manipulation because light can be easily reconfigured with a high spatial resolution (up to the diffraction limit) and instantaneous response. Experimental studies have successfully demonstrated manipulation of micro/nano particles²², liquid drops^{23,24}, Janus drops²⁵ and solid swimmers²⁶ in liquids; theoretical work has elucidated the link between light-induced surface tension changes and the resulting flow fields, for applications including translating drops and large interfaces^{27,28}. However, many practical multi-phase applications such as boiling, condensation, microfluidic-based synthesis, and

electrocatalysis require removing bubbles and droplets from a solid surface, which has not been investigated using photo-responsive surfactants, to the best of our knowledge.

In this study, we introduce the use of photo-responsive surfactants to promote bubble and droplet departure from a solid surface. We employ a photo-responsive surfactant that we recently designed and synthesized²⁹, which is capable of achieving fast, reversible, and significant interfacial changes of different solvents, thanks to its large polarity change under illumination. To highlight the potential of this approach, we demonstrate the removal of droplets and bubbles pinned on a solid substrate using dilute (0.1 mM) photo-responsive surfactants and low-intensity (0.25 mW/mm²) lights. This is achieved by creating a net force on the bubble or droplet due to the Marangoni effect induced by the non-uniform distribution of these photo-responsive surfactants (Figure 1b). Since light is used to induce Marangoni stresses, we refer to this effect as “photo-Marangoni”. In particular, we demonstrate that the departure of an otherwise stably pinned droplet can occur in less than 0.4 s. For pinned air bubbles, the departure volume can be reduced by 20%, indicating that departure is significantly accelerated. Numerical simulations are performed to understand the dominating factors contributing to the bubble and droplet departure. The physical insights on fundamental fluid manipulation gained in this study have broad potential applications, such as drug delivery, boiling heat transfer, and electro-catalysis.

Scaling estimates of photo-Marangoni effects in drop/bubble departure

To estimate the potential significance of photo-Marangoni forces in the depinning of drops and bubbles, we perform order-of-magnitude estimates. For this purpose, it is useful to briefly review the underlying molecular mechanisms.

Photo-responsive surfactants are synthesized by covalently attaching a photo-switchable molecule to a surfactant carrier³⁰. The photo-switchable moiety can exist as two different isomers. The first isomer is thermodynamically stable in the dark, but will undergo a conformational switch to the meta-stable isomer initiated by illumination of a specific wavelength (Figure 1a). If illumination is stopped or a different wavelength of light is applied, the isomer can revert back to the thermodynamically stable form. The reversible photo-conversion is associated with a change of surface tension or interfacial tension γ of the surfactant-containing solution (Figure 1a).^{31,32}

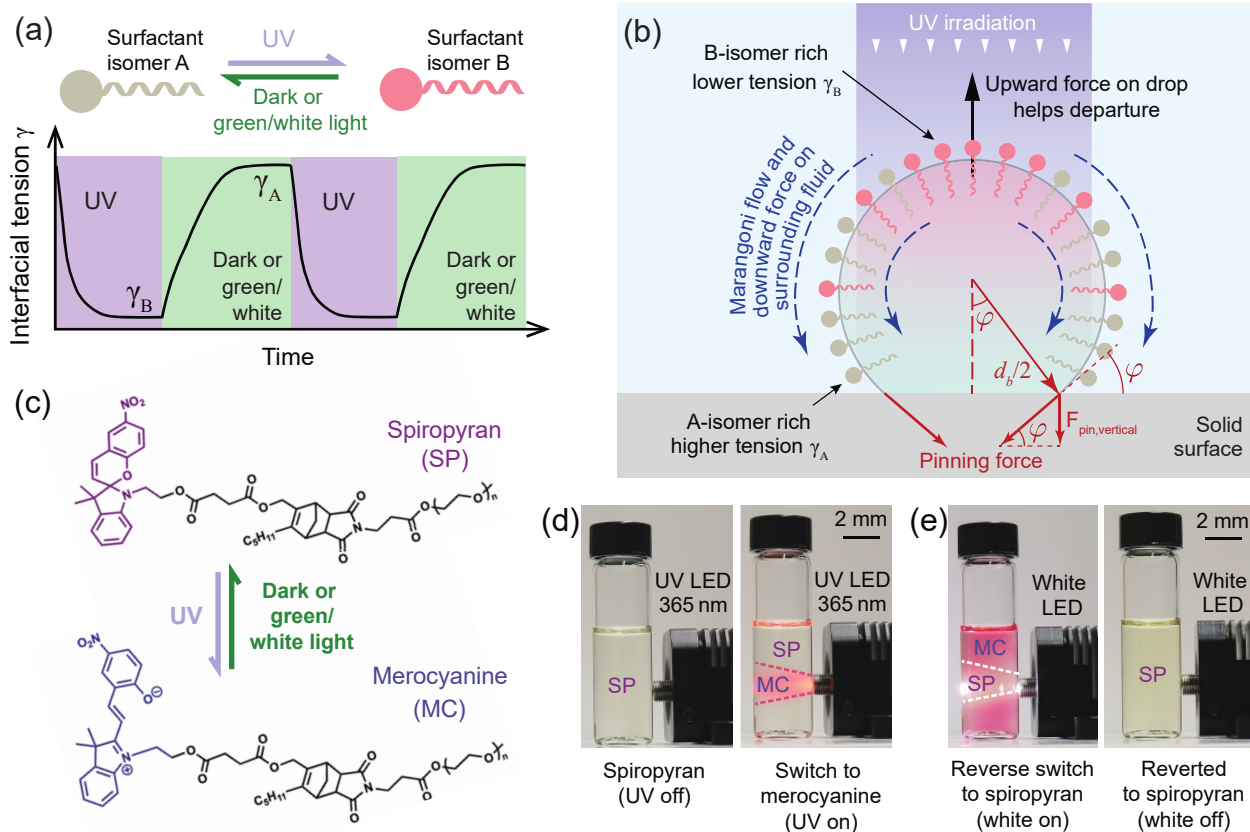


FIG. 1. Mechanism of photo-Marangoni effect for light-activated bubble/droplet departure. (a) Photo-responsive surfactants reversibly switching molecular conformation upon illumination of light with appropriate wavelengths. In this example, forward switching is activated by UV light. The reverse reaction occurs once UV is removed, and is accelerated by green light or white light. The surface tension is changed reversibly by UV/green illumination. (b) A surface tension gradient can be established along the interface by applying light with an intensity gradient, or only to one region on the interface. The subsequent Marangoni flow drives the bubble/droplet to depart. (c) The reversible photo-conversion of the spiropyran (SP) isomer to the merocyanine (MC) isomer form. (d) 0.1 mM spiropyran water solution changes from transparent to light pink under 365 nm UV illumination. (e) 0.1 mM spiropyran water solution switches from MC form back to SP form, as shown by the color change from light pink to transparent.

Applying light to only one side of a single bubble or droplet whose surface is covered with photo-responsive surfactants (Figure 1b) causes a localized photo-reaction and induces a change of γ at the interface between the two fluids, which drives a local Marangoni flow toward the region of higher γ . The Marangoni flow pushes surrounding fluid (downward in Figure 1b), such that the bubble/droplet experiences a Marangoni-induced force F_M in the opposite direction, easing the depinning and departure from the substrate (the fluid mechanics of generic Marangoni-induced

droplet propulsion are reviewed in Ref. ¹³). We propose here that, if a gradient in γ can be tuned and sustained by maintaining a constant gradient of two photo-switched isomers, bubbles and droplets can be continuously removed from the solid substrate on-demand.

To estimate the relative change of surface tension $\Delta\gamma/\gamma$ that is required to depin an air bubble immersed in an aqueous solution (Figure 1b), we consider the relative order of magnitude of the relevant forces. For a static bubble pinned to a substrate, the bubble diameter d_b at departure from a substrate is obtained by balancing buoyancy F_b , which is of order $g\Delta\rho d_b^3$ (where $\Delta\rho$ is the density difference), and the vertical component of the pinning surface force $F_{pin,vertical} \sim \gamma d_b \sin^2\varphi$ (where φ is the macroscopic or apparent contact angle in the liquid, and “ \sim ” denotes order of magnitude), yielding $d_b \sim \sin\varphi(\gamma/g\Delta\rho)^{1/2}$. Here, the pinning force (Figure 1b) originates from the surface tension γ multiplied by the contact line length $\pi d_b \sin\varphi$, which results in a vertical component of $F_{pin,vertical} \sim \gamma d_b \sin^2\varphi$. For photo-Marangoni forces to assist departure, they must be non-negligible by comparison to buoyancy for a bubble of size d_b or smaller. If a surface tension change of order $\Delta\gamma$ exists across the height of the bubble, and can be maintained to drive a flow, the resulting photo-Marangoni force that can assist depinning is of order $\Delta\gamma d_b$; requiring this to be at least 10% of the buoyancy force sets $\Delta\gamma \gtrsim 0.1g\Delta\rho d_b$. In the extreme case of microgravity applications, or of immiscible fluids with matched densities, the photo-Marangoni force alone must overcome the totality of the pinning surface force $F_{pin,vertical}$, which requires $\Delta\gamma \gtrsim \gamma \sin^2\varphi$. These order-of-magnitude estimates inform our choice of photo-responsive surfactant, as explained below.

Characterization of SP-DA-PEG

An ideal surfactant to achieve bubble departure in a multi-phase system should display a large surface tension change, good reversibility, fast switching kinetics activated by a low-intensity light. As such, we designed and synthesized^{29,33} (Supplementary Information) a spiropyran-based photo-isomerizable molecule (SP-DA-PEG) using a recently developed, norbornadiene enabled Diels–Alder (DA) click chemistry^{33,34}. As shown in Figure 1c, SP-DA-PEG comprises the photo-switchable spiropyran unit at the surfactant tail and the poly(ethylene glycol) monomethyl ether (PEG, $M_n \approx 550$ g/mol) chain as the hydrophilic head group on which spiropyran is immobilized. The surfactant design enables the largest change in polarity upon photo-switching as the initially amphiphilic molecule loses its hydrophobicity upon irradiation. The isomerization of the

spiropyran (SP) isomer to the merocyanine (MC) isomer is activated by UV light (300-375 nm), whereas the reverse photo-isomerization occurs upon the removal of UV irradiation, which can be further accelerated by application of visible light (500-600 nm)^{23,31} (Figure 1c). In Figure 1d, the color of a 0.1 mM spiropyran water solution changes from transparent to light pink upon irradiation of 365 nm UV light, using a low-power fiber coupled UV LED. The region not illuminated by the UV light remains transparent. After illuminating the entire solution with a high intensity UV lamp, which turns the solution pink (MC isomer), we illuminated the solution using a fiber-coupled white LED (Figure 1e). This quickly generated a clear region, which indicates the fast reverse reaction of MC to SP under white light. All MC isomers are completely transformed back to SP in the right-hand image of Figure 1e. In previous work, we explored the photo-wetting behaviors of SP-DA-PEG and revealed the excellent reversibility and stability of SP-DA-PEG at oil/water interfaces by examining both the kinetics and interfacial tensions²⁹. Compared with many previously reported photo-responsive surfactants, the ease of synthesis and well-studied properties of SP-DA-PEG make it an ideal candidate for the manipulation of fluid systems explored in this work.

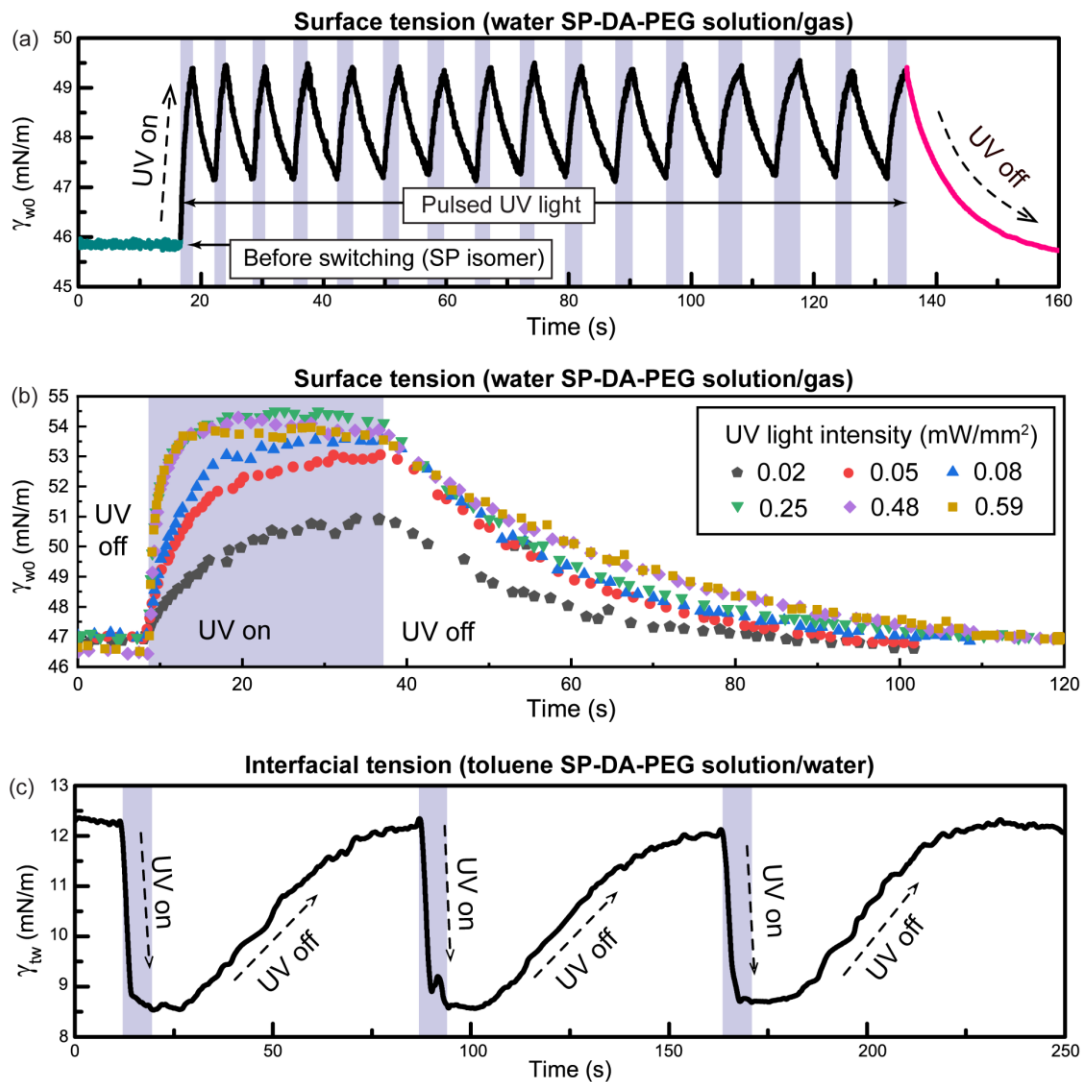


FIG. 2. Reaction kinetics of SP-DA-PEG isomerization. (a) The surface tension of 0.1 mM SP-DA-PEG water solution under repetitive pulsed UV light. (b) The surface tension of 0.1 mM SP-DA-PEG water solution under UV irradiation with different light intensity. (c) The reversible change of interfacial tension between 0.1 mM SP-DA-PEG toluene solution and DI water.

We measured the surface tension response of SP-DA-PEG solutions during photoisomerization using the pendant drop method³⁵ on a commercial tensiometer (Theta Flex, Biolin Scientific). Although an accurate measurement of interfacial/surface tensions of surfactant solutions can be challenging, as the timescales for surfactants to diffuse to the interface and for the droplet to relax to full equilibrium can take tens of minutes³⁶, these pendant drop measurements are directly relevant to depinning applications, where timescales are inherently much shorter than those associated with molecular diffusion.

First, we applied alternating irradiation of 365 nm UV and white light to an aqueous SP-DA-PEG solution (0.1 mM), and observed the response of an air bubble. In Figure 2a, γ_{w0} quickly rises to 49.5 mN/m from 46 mN/m after 1 second of UV irradiation. Once UV is removed and the white light is applied, γ_{w0} undergoes a rapid decrease. After 16 cycles of irradiation, γ_{w0} can recover its original value, which indicates that spiroiran could potentially maintain its performance through large numbers of depinning cycles.

Figure 2b shows the time evolution of γ_{w0} of 0.1 mM aqueous SP-DA-PEG solution under different light intensities. At the smallest intensity of 0.02 mW/mm², γ_{w0} changes from 46.5 mN/m to around 50.4 mN/m in 38 seconds. When light intensity is increased, more SP molecules are transformed into the open-ring conformation, MC, at a faster rate and the resultant surface tension is increased to 54.3 mN/m within 8 seconds. In addition, most SP molecules can be converted into the open-ring form and the photo-conversion process saturates once the light intensity exceeds 0.25 mW/mm², which is still a relatively low intensity in most optical applications. After the UV light is removed, γ_{w0} reverts to its original value for all cases.

We also measured the dynamic response of the interfacial tension γ_{tw} between deionized (DI) water and a 0.1 mM SP-DA-PEG toluene solution, as shown in Figure 2c. Under 365 nm UV light with intensity of 0.59 mW/mm², γ_{tw} quickly changes from 12.33 ±0.05 mN/m (SP) to 8.59 ±0.10 mN/m (MC), corresponding to a 30% change.

Droplet departure experiments

We carried out experiments on the departure of a liquid droplet, consisting of toluene, in water. The experimental setup is shown in Figure 3a. A toluene droplet is injected into a water bath through a round hole ($d = 0.61$ mm) using a syringe pump to control the injection rate. The droplet contains 0.1 mM SP-DA-PEG; this concentration showed the most significant interfacial tension change through our pendant drop experiments. The droplet is stabilized at ~15 μ L (corresponding to a diameter of approximately 3 mm) and remains pinned to the hole (Figure 3b). Later, another equal-sized droplet is generated and equilibrated for 10 s. Then, the output from a multiline Argon Ion UV laser (351.1+363.8 nm, beam diameter of 1.3 mm) is directed to the top of the droplet (height of 3.5 mm). The incident light intensity on the droplet is 44 mW/mm², as measured in the empty container. The laser enables precise targeting of the photoswitch, and the higher intensity accelerates the isomerization to MC.

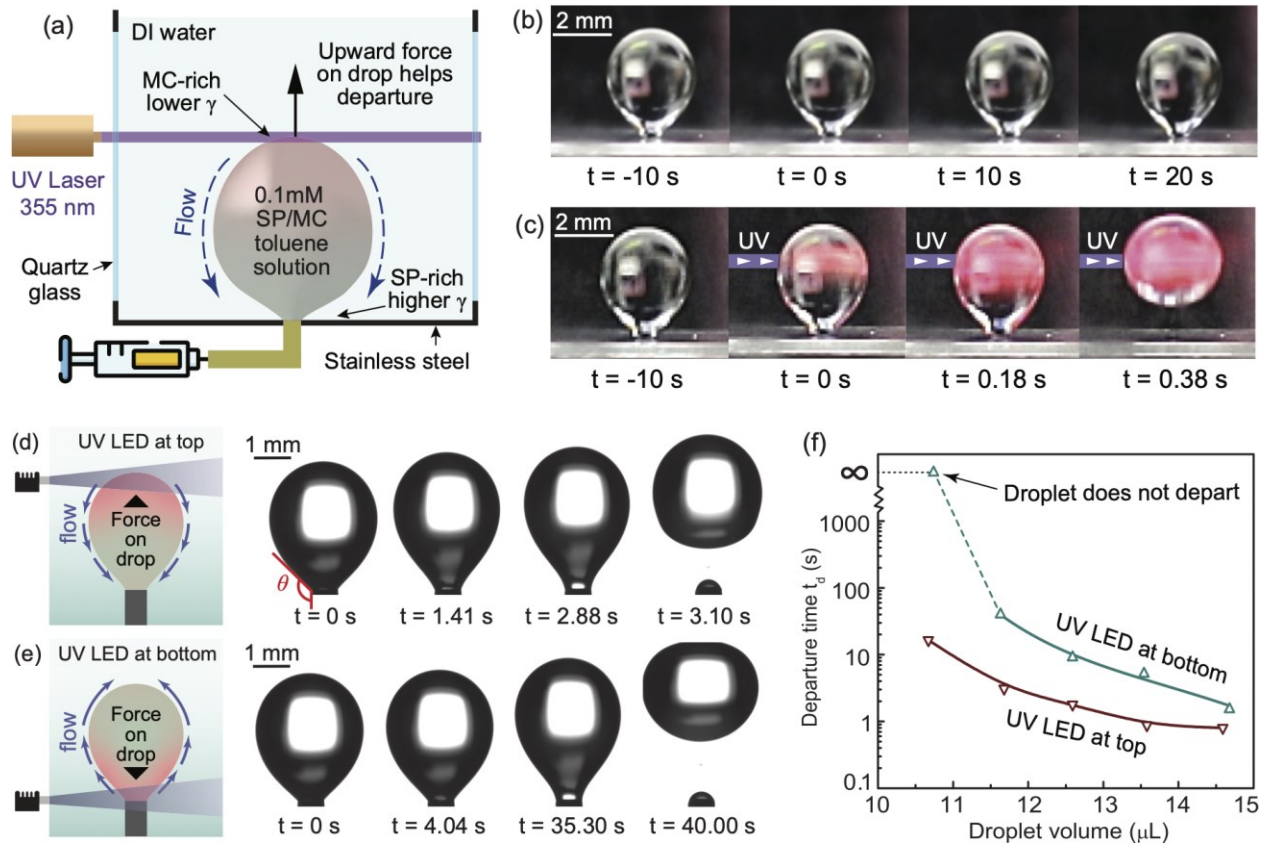


FIG. 3. Droplet departure activated by UV laser and LED. (a) Schematic of the experimental setup of laser-activated droplet depinning. A $\sim 15 \mu\text{L}$ droplet is generated by pushing the toluene solution with 0.1 mM SP-DA-PEG through a hole (0.61 mm in diameter). A collimated UV laser is directed at the top part of the droplet to trigger the photo-Marangoni effect. Experimental results show that (b) without UV laser illumination, a $\sim 15 \mu\text{L}$ droplet stays static, and (c) with UV laser illumination, a $\sim 15 \mu\text{L}$ droplet departs in only 0.38 s. (d) The photo-Marangoni effect facilitates the depinning of a toluene droplet ($\sim 11.5 \mu\text{L}$) when the droplet top is irradiated by a low-intensity UV LED. The depinning time t_d is 3.10 s. (e) When the UV LED illuminates the bottom of a same sized toluene droplet, the photo-Marangoni effect suppresses the departure of the droplet by creating an upward Marangoni flow. The depinning time t_d increases to 40.00 s. (f) The depinning time t_d of droplets when illuminated with a UV LED as a function of droplet volumes. t_d becomes orders of magnitude higher when UV irradiation is applied at the droplet bottom.

Figure 3c demonstrates that the initially pinned toluene droplet departs the substrate in only 0.38 s after UV irradiation (Supplementary Movie 1). We define the instance when the laser is turned on as $t = 0$ s. A pink region rapidly forms within the top part of the droplet where the UV beam passes through, indicative of the onset of the photo-conversion. The widening of the pink region observed at $t = 0.18$ s suggests fluid flow from the pink MC-rich lower interfacial tension region to the clear SP-rich higher interfacial tension region. The fluid motion inside the toluene

droplet is demonstrated by visual inspection of tracer particles (Supplementary Movie 2 and 3). The detailed flow field and force analysis will be discussed in the following sections. To ensure that droplet departure is activated by photo-Marangoni effect rather than the possible thermal-Marangoni effect induced by laser heating within the droplet, we simulated the temperature rise ΔT within the toluene droplet (see Supplementary Information). It is found that ΔT is limited to only 0.25 °C before droplet departure ($t = 0.38$ s). In addition, the droplet temperature is experimentally measured to have increased from 21.7 ± 0.1 °C to 23.2 ± 0.8 °C during 17 seconds of laser heating (see Supplementary Information). A previous work demonstrated that γ_{tw} for water/toluene decreases by 1.8% when the temperature is increased from 20 °C to 25 °C³⁷. Therefore, thermal Marangoni effects are negligible in this experiment. This estimate also illustrates the advantage of the photo-Marangoni effect over thermal Marangoni, in that a much smaller light intensity can manipulate multi-phase flow without the need to generate a substantial temperature gradient in the droplet. Furthermore, the light intensity used for photo-Marangoni experiments (44 mW/mm²) is 2-4 orders of magnitude lower than those previously reported for thermal Marangoni examples^{38,39}.

We further demonstrate that droplet departure can be activated with even lower light intensity, and that the time for droplet departure t_d shows a strong dependence on droplet size. Here t_d is defined as the time of droplet departure after UV irradiation. In this second set of experiments, we use a fiber-coupled UV LED with a light intensity of only 0.59 mW/mm² (this is nearly 75 times smaller than in our experiments with the UV laser). A computer-controlled droplet dispenser is used to generate a toluene droplet with precisely controlled volume. As before, the droplet contains 0.1 mM SP-DA-PEG and is immersed in DI water. The UV LED illuminates the top part of a 11.5 μ L droplet, as shown in Figure 3d. As a result, γ_{tw} locally decreases and a downward Marangoni flow drives the droplet to depart after 3.10 s. By contrast, a reverse-direction photo-Marangoni flow can be generated by illuminating the bottom part of the droplet with the UV LED (Figure 3e, Supplementary Movie 4). This reverse photo-Marangoni flow hinders droplet departure, as shown by the fact that t_d increases by an order of magnitude ($t_d = 40.0$ s). The droplet eventually still departs the surface; a contributing factor of this departure may be the reduced pinning force F_{pin} as a result of the decreased interfacial tension γ_{tw} after the photo-conversion. As shown in Figure 2c, photo-conversion will cause γ_{tw} to decrease by 30%. As the pinning force is proportional to γ_{tw} , the buoyancy may eventually be able to overcome the pinning force and the

downward photo-Marangoni force. In Figure 3f, we measured the depinning time t_d for toluene droplets with different volumes. As the droplet volume increases, t_d decreases exponentially due to increased buoyancy; yet the departure time is significantly shorter for droplets with UV applied at the top than at the bottom for all droplets tested.

Bubble departure experiments

In this section we show that the photo-Marangoni effect can also be used to assist the departure of air bubbles. The assisted departure is demonstrated by a reduction in the maximum bubble volume V_d before departure. Figure 4a shows the experimental setup. A syringe pump is used to generate an air bubble in a chamber filled with 0.1 mM SP-DA-PEG in toluene solution. The same UV LED used for the droplet experiments illuminates from 2.5 cm above the bubble. The highly diverging feature of its light naturally creates a light intensity gradient in the vertical direction along the bubble. Furthermore, a 532 nm green laser shines a beam horizontally at the bottom of the bubble. The green light irradiation accelerates reverse isomerization from MC to SP and subsequently enhances the composition gradient of surfactants along the interface. In turn, this increases the surface tension difference across the bubble. In our previous work²⁴, it was found that the surface tension of SP-DA-PEG toluene solutions (γ_{t0}) decreases after the photo-isomerization from SP to MC. Therefore, the bubble top is rich in MC and has a lower surface tension, leading to a downward photo-Marangoni flow which drives the bubble to depart. Using the pendant drop method, γ_{t0} is measured to reduce slightly from 23.25 mN/m to 22.75 mN/m upon UV irradiation, a modest change (only 2%) compared to that of γ_{tw} .

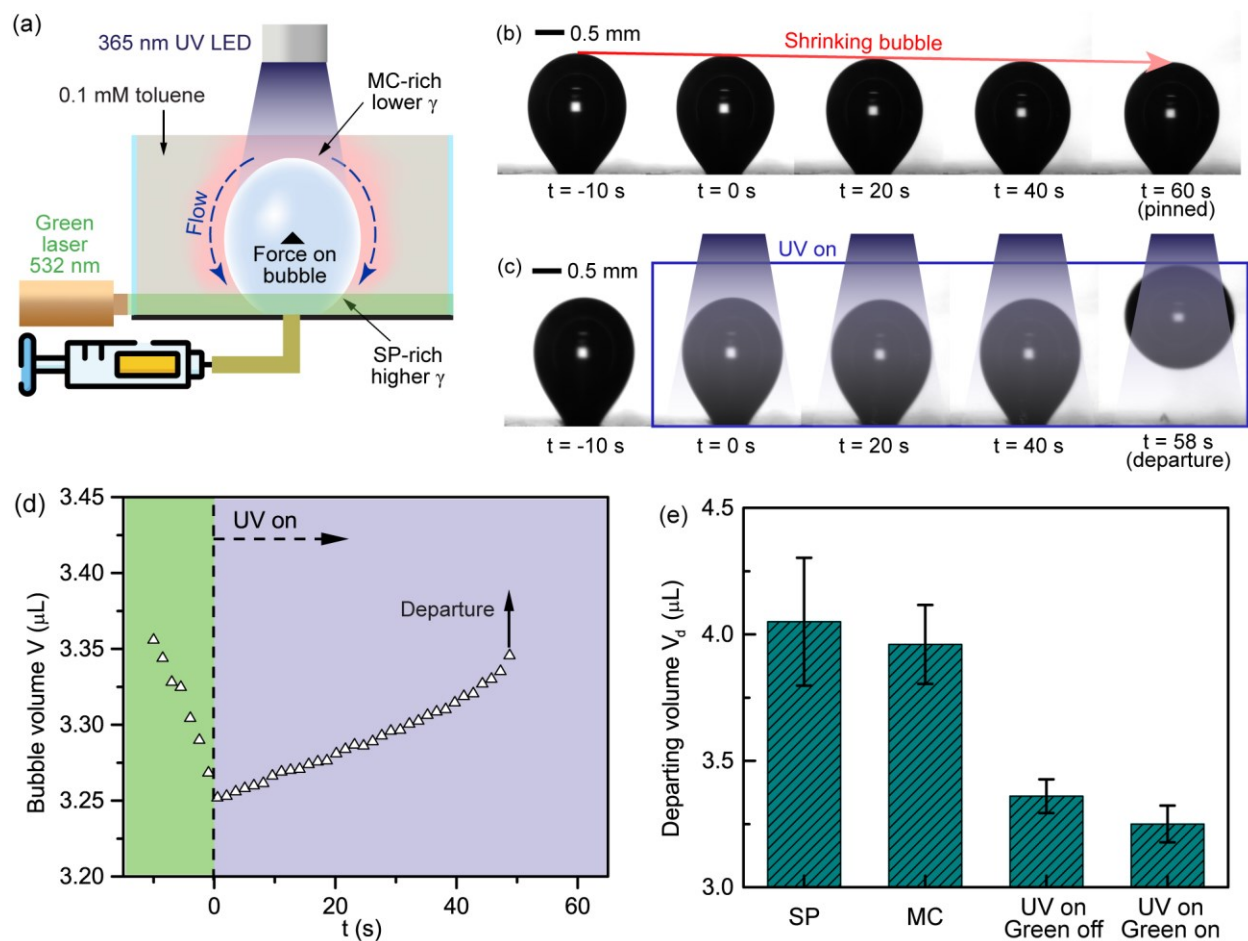


FIG. 4. Departure of an air bubble incurred by the Photo-Marangoni effect. (a) Schematic of the experimental setup in the bubble experiment. The photo-Marangoni effect is driven by a UV LED illuminating downwards from 2.5 cm above the bubble, and it is further assisted by a collimated green laser beam shining near the bottom of the bubble. Together, these enhance the difference in isomer composition across the bubble, and thereby increase the surface tension difference. (b) A pinned air bubble ($\sim 3.36 \mu\text{L}$) naturally shrinks in toluene solution, and fails to depart. (c) An air bubble of the same initial volume leaves the surface under the photo-Marangoni effect. (d) The volume change of an air bubble before and after UV irradiation; departure occurs at a volume that is smaller than the initial one. (e) The bubble volume at departure V_d in SP solution, MC solution, SP solution when UV LED is on and green laser is off, and SP solution when UV LED and green laser are both on.

We compared V_d for bubbles injected into SP solutions, MC solutions, and solutions with a mixture of SP and MC isomers by controlling the illumination conditions. Time-lapse images of the injected bubble immersed in 0.1 mM SP-DA-PEG toluene solution when no light is applied are shown in Figure 4b. At $t = -10$ s, the syringe pump is stopped and the bubble remains pinned to the surface. A slow shrinkage is observed over a period of 60 s, which is likely due to a small

imperfection in the seal of the gas supply line. In contrast, when UV LED is turned on (at $t = 0$ s) for an equal-sized bubble generated with the same method (Figure 4c), the originally shrinking bubble starts to inflate as the photo-Marangoni lift force is applied, and departs from the surface at $t = 58$ s. The time-dependent volume of the bubble during this process is shown in Figure 4d. The thermal Marangoni effect is negligible as the solution temperature is measured to increase by only 0.5 °C during 1 minute of UV irradiation (see Supplementary Information). Bubble departure volumes for SP-only solutions $V_{d,SP}$ and for MC-only solutions $V_{d,MC}$ are measured by generating a quasi-steady-state bubble using the syringe pump with a constant and low flow rate of 1 $\mu\text{L}/\text{min}$. It is found that $V_{d,SP} = 4.05$ μL and $V_{d,MC} = 3.96$ μL . The difference between $V_{d,SP}$ and $V_{d,MC}$ agrees well with surface tension change of 0.1 mM SP-DA-PEG toluene solution before and after the photo-isomerization. The bubble departure size can further be reduced to $V_{d,UV,G} = 3.25$ μL (Figure 4e) by applying UV and green light (5 mW) to the top and bottom of the bubble, respectively, as illustrated in Figure 4a. The photo-Marangoni force F_M , as a percentage of the buoyancy force, herein is evaluated to be $F_M/F_B \cong (V_{d,SP} - V_{d,UV,G})/V_{d,SP} = 19.8\%$, even with a modest change (2.1%) of surface tension of SP-DA-PEG solution. The above equation assumes that the bubbles are in quasi-static states and that the pinning force is relatively the same for all the cases. By designing new surfactants and characterizing the surface tension change in different solvents, the photo-Marangoni effect acting on gaseous bubbles can potentially be further enhanced.

Finite element simulations

We carried out several finite element simulations to investigate the lift force due to the photo-Marangoni effect (details in Methods), focusing on toluene droplets in DI water. We first simulate the departure of a 10.65 μL droplet (0.1 mM SP-DA-PEG) and assume a linear interfacial tension gradient with $\gamma_{\text{top}} = 8.59$ mN/m at the top of the droplet and $\gamma_{\text{b}} = 12.33$ mN/m at the bottom. These values are based on the assumptions that the photo-conversion equilibrium is established (Figure 2c) and the proportions of SP and MC molecules are determined by the local light intensity, which we will further discuss. Figure 5a presents the velocity field in both phases when the photo-Marangoni effect is activated. Within the droplet, the liquid travels downward near the interface due to the Marangoni stress and then circulates back to the top near the center axis. Outside the droplet, there is also a downward flow which moves faster at the interface and decays to almost

zero away from the droplet. The pressure distribution is shown in Figure 5b. A high-pressure region appears near the base of the droplet in the outer phase, due to the stagnant flow near the bottom wall. This high-pressure region exerts an additional lift force on the droplet. Figure 5c plots the profiles of the z-component of total stress σ_z , viscous stress τ_z , and pressure p_z from the droplet bottom to its top. Interestingly, the result shows that pressure is the dominating factor near the bottom of the droplet, but then dips at a height below the maximum width of the droplet, slightly hindering departure. In contrast, the profile of τ_z is relatively flat, indicating that the outer phase is constantly pushing the droplet upward through surface shear.

However, the above simulation may be over-predicting F_M , since it assumes that the maximum possible interfacial tension difference is realized across the drop, whereas in practice the finite-time kinetics of the photo-conversion may not allow the MC-isomer to fully switch back to the SP-isomer before the fluid reaches the bottom of the droplet. Therefore, we reduced the interfacial tension difference and calculated the corresponding photo-Marangoni force F_M , looking for the minimum interfacial tension difference that would enable departure. Since the forward reaction is fast (Figure 2c), we fixed γ_{top} at 8.59 mN/m by assuming a complete photo-conversion under UV irradiation, and gradually increased γ_b , corresponding to a decreasing proportion of MC molecules in the surfactant mixture. Figure 5d summarizes the upward force contributed by pressure F_p and viscous stress F_v under different $\Delta\gamma/\gamma_0$, where $\Delta\gamma = \gamma_b - \gamma_{\text{top}}$ and γ_0 is the interfacial tension before the photo-conversion. F_p and F_v are of the same order of magnitude for $\Delta\gamma/\gamma_0$ spanning from 0% to 30%, indicating that both pressure buildup at the bottom and the relatively constant viscous shear contribute substantially to the photo-Marangoni force F_M . In Figure 2b, we have shown that the interfacial response of SP-containing solutions can be tuned by adjusting the UV light intensity. Therefore, the UV intensity can be used not only in depinning an originally pinned droplet, but also to tune the net force acting on the droplet and the subsequent departure dynamics. Note that as F_p and F_v increase with respect to $\Delta\gamma/\gamma_0$, the net photo-Marangoni force $F_M = F_p + F_v$ eventually exceeds buoyancy F_B at $\Delta\gamma/\gamma_0 = 29.4\%$. This suggests that the photo-Marangoni effect could even serve to completely replace buoyancy forces if using two density-matched fluids, or if working in microgravity environments. The net force F_N on the droplet can be estimated by considering the pinning force $F_{\text{pin}} = \pi d_s \gamma_b \sin\theta$, buoyancy $F_B = \Delta\rho gV$, and the photo-Marangoni force F_M , such that $F_N = F_M + F_B - F_{\text{pin}}$. In Figure 5e, it is shown that F_M is of the same order of magnitude as F_B . For small $\Delta\gamma/\gamma_0$, F_N is negative, indicative of a pinned droplet on the substrate;

droplet departure ($F_N > 0$) occurs when $\Delta\gamma/\gamma_0$ exceeds 21.5%. Therefore $\Delta\gamma/\gamma_0$ required for departure is below the maximum $\Delta\gamma_{\max}/\gamma_0 = 30\%$ that we previously measured in our tensiometer experiments, which further supports the feasibility of photo-Marangoni-assisted departure.

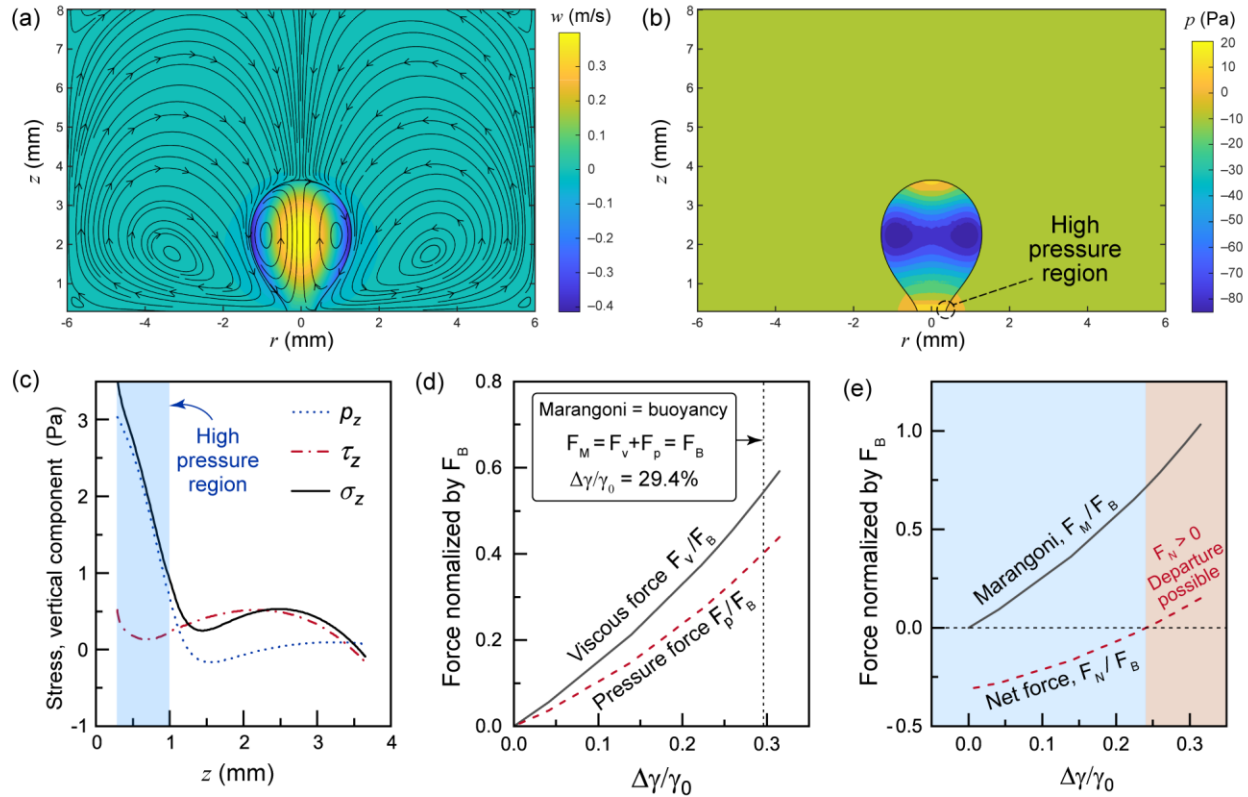


FIG. 5. Computational results of light-activated droplet departure enabled by the photo-Marangoni effect. (a) The streamline plots and w -velocity contour and (b) pressure contour around the droplet when the photo-Marangoni effect is activated. (c) The distribution of z -stresses acting on the droplet along the droplet interface. P_z is the vertical component of the pressure, τ_z is the viscous stress, and σ_z is the total stress. All quantities are positive if they push the drop upward. (d) The force contributed by pressure and viscous stress normalized by the buoyancy F_B . $\Delta\gamma$ is the difference between γ_b and γ_{top} , and $\gamma_0 = 12.33$ mN/m is the interfacial tension before the photo-conversion. (e) The Marangoni force F_M and net force F_N versus different interfacial tension gradients. $F_N = 0$ is achieved at $\Delta\gamma/\gamma_0 = 21.5\%$.

Discussion and conclusions

In summary, we developed a dynamic, non-invasive and sustainable manipulation scheme to enable bubble and droplet departure from solid surfaces using a light-responsive surfactant, namely SP-DA-PEG. The excellent reversibility, stability, sensitivity to illumination, as well as fast photo-isomerization kinetics make SP-DA-PEG ideal for applications involving bubble and

droplet manipulation. In our experiments, an interfacial tension change as high as 30% and a droplet departure time of 0.38 s (for an otherwise pinned droplet) are achieved. Both experiments and simulations demonstrate that the photo-Marangoni force arises not only from the viscous shear along the interface, but also from the pressure build-up due to flow stagnation at the bottom. As a matter of fact, the photo-Marangoni flow induces a Reynolds number (based on interface velocity, drop diameter and ambient fluid properties) of approximately 600, indicative of a laminar flow where inertial effects may not be negligible. Therefore, even a modest change in surface tension (2.1%) can lead to a significant change in bubble behaviors (19.8% change in bubble departure volume). Note that the insights gained from the simulations can be extended to describe other photo-responsive surfactants and interfaces which may have a different interfacial response upon illumination. While the interfacial tension may increase or decrease upon illumination, as long as a downward Marangoni flow is generated, a lift force can be created to assist bubble/droplet depinning. Therefore, the depinning dynamics will remain unchanged. The photo-Marangoni effect can serve as an effective yet simple platform technology for non-invasive dynamic fluid manipulation that does not require electrical voltage, magnetic field, patterning complex electrodes or engineering of well-designed surface textures. The surfactant concentration used in this work is around 0.1 mM, which is even smaller than the concentration of natural or man-made surfactants in environmental water⁴⁰. The required light intensity for complete photo-isomerization is only around 0.25 mW/mm², comparable to the average solar irradiance received by the earth's surface⁴¹. Therefore, the photo-Marangoni effect can contribute to developing new research capabilities not only in applications requiring fluid removal such as heat transfer, electrolysis, organic synthesis, but also in processes that entail biological compatibility and optical resistance, such as biochemical assays, dynamic patterning and manufacturing of novel materials. Furthermore, the physical insights gained in the theoretical analysis, experimental observations and numerical simulations will guide the design and synthesis of photo-surfactants for future photo-driven multi-phase systems.

More work can be done to improve the photo-Marangoni effect to achieve faster response and more durable performance. The mechanism of interfacial tension change during photo-conversions depends on the ring-opening process of the photo-switch unit, resulting in a polarity change and charge redistribution of SP-DA-PEG. Typically, the effect of spiropyran-based surfactants on non-polar interfaces, such as the toluene-air interface, becomes less significant

compared to that of an interfacial system involving polar liquids like water. Therefore, the meticulous design and optimization of molecular structures of the light-responsive surfactants is needed to achieve optimal interfacial tension change and reaction kinetics for different combinations of interfacial systems. In addition, more detailed numerical and theoretical studies on the coupling between multiphase flow, interface deformation, species transport, surfactant adsorption, and photo-reactions can provide more insights to explore the surfactant transport and fluid dynamics associated with the photo-Marangoni effect for optimal performance.

Methods

Synthesis of SP-DA-PEG. SP-alcohol⁴² and NBD-COOH³³ were synthesized following literature procedures, and mal-PEG was prepared from commercially available poly(ethylene glycol) monomethyl ether (PEG, $M_n \approx 550$ g/mol) functionalized with 3-maleimidopropionic acid as previously described³³. Norbornadiene functionalized spiropyran (SP-NBD) was prepared by first dissolving SP-alcohol (1.0 eq) in anhydrous dichloromethane (DCM, 0.1 g/mL). To this solution was added and NBD-COOH (1.2 eq), 1-Ethyl-3-(3-dimethylaminopropyl)carbodiimide (1.5 eq) and 4-dimethylaminopyridine (0.10 eq). The resulting mixture was allowed to stir for 24 h, then washed with water, dried over magnesium sulfate, and concentrated to afford a residue that was purified on a plug of silica. The residue was first rinsed with hexanes, then eluted from the silica plug with a mixture of ethyl acetate and hexanes (5:95). The organic solvent was removed under reduced pressure to afford SP-NBD as a viscous pink/green oil (61%) that was used in a one-pot deprotection to SP-cyclopentadiene and DA click to mal-PEG. To accomplish the one-pot DA click, SP-NBD (1.4 eq), mal-PEG (1.0 eq) and 3,6-di-2-pyridyl-1,2,4,5-tetrazine (2.0 eq) were dissolved in chloroform (0.1 g/mL) and allowed to stir for 15-24 h. Reaction completion was determined by ¹H NMR of the crude reaction mixture in deuterated chloroform. Upon disappearance of the maleimide protons (6.7 ppm) – indicating complete conversion of mal-PEG to SP-DA-PEG – norbornylene (2.0 eq) was added to the solution to quench remaining tetrazine and facilitate purification. After stirring an additional 30 min, the solution was passed directly through a silica plug. The material was first rinsed with DCM to remove the yellow byproduct, then the pink product was eluted with a mixture of methanol in DCM (1:9). The solvent was removed under reduced pressure and the residue taken up in ethanol (25 mL/g polymer). The solution was transferred into centrifuge tubes and cooled in a dry ice/acetone bath (-78 °C) before

the functionalized polymer was isolated by cold centrifugation. The supernatant was decanted from the pink pellet and the cold ethanol precipitation and centrifugation was repeated once more. The resulting pink polymer pellet was redissolved in DCM, then dried under reduced pressure to afford the desired SP-DA-PEG (48%) as green/pink viscous liquid. $M_n(\text{NMR}) = 1300 \text{ g/mol}$. Further synthetic detail and characterization of SP-DA-PEG can be found in the Supplementary Information.

Sample preparations. The photoactive surfactant selected for this work is a spiropyran-based photo-isomerizable molecule (SP-DA-PEG). SP-DA-PEG can easily dissolve into toluene liquids by vortexing and sonication.

Light sources. In the bubble experiment, a custom-built multiline Argon Ion UV laser (351.1+363.8 nm, beam diameter of 1.3 mm) is used with a beam diameter of 1.3 mm and light intensity of 44 mW/mm^2 . The fiber-coupled UV LED and white LED are directly bought from Thorlabs, Inc. (M365FP1-365 nm, 9.8 mW Fiber-Coupled LED, and MCWHF2-6200 K, 21.5 mW Fiber-Coupled LED) A high intensity UV lamp (100 W over a lamp area of $216 \text{ mm} \times 140 \text{ mm}$, UVP High Intensity Lamp, Analytik Jena) is used to fully transform the SP isomers in 0.1 mM SP-DA-PEG solutions into the MC isomers so as to measure the bubble departure volume in pure MC solutions. A 532 nm green laser (5 mW, GMY-532-5F3-PP, Lasermate Group, Inc) is used to expedite the reverse photo-isomerization of SP-DA-PEG molecules in the bubble experiment.

Droplet and bubble experiments. A stainless steel tube with four glass windows is fabricated using the CNC milling machine and a round hole with a diameter of 0.6 mm is fabricated at the tube bottom using a mechanical drilling rig. The round hole is connected to a syringe pump and sealed by Dow Corning High Vacuum Grease. All experimental glassware are cleaned by sonication in water and isopropyl alcohol to prevent contamination by residual surfactant molecules and dust. Droplet is equilibrated for about 1 min before recording. For droplet manipulation with UV LED, the LED is placed about 2 cm away from the side of the droplet. For the bubble experiment, the UV LED is mounted around 2 cm above the air bubble. Videos are recorded from the side using Canon EOS 80D.

Pendant drop measurements. All measurements related to the surface tension or interfacial tension were carried out on the Theta Flex Tensiometer from Biolin Scientific. This instrument uses a high-speed camera to capture the outline of drops and bubbles. The pendant drop method is then used to calculate the surface tension or interfacial tension dynamically.

Particle tracing. To demonstrate the flow pattern inside the toluene droplet, we added conductive silver-coated hollow glass microspheres (900 kg/m^3 , $25\text{-}65 \text{ }\mu\text{m}$, Cospheric LLC) into 0.1 mM toluene solutions before filling into the syringe. The particle-containing solution is then injected into DI water and the droplet volume is tuned to make sure the droplet stays pinned after UV irradiation. The particle density is close to that of the toluene solution such that the effect of gravity or buoyancy on the motion of those microspheres is negligible. The Argon Ion UV laser was used to trigger the photo-Marangoni flow within the droplet and all video frames were recorded using the Canon EOS 80D.

Finite element simulations. We capture the outline of the droplet right before it departs and assume that the droplet is in a quasi-steady state. The computational domain is axisymmetric ($6 \text{ mm} \times 12 \text{ mm}$) and the flow is laminar due to low Reynolds number. The governing equations are continuity and Navier-Stokes equations:

$$\begin{aligned}\nabla \cdot (\rho \vec{u}) &= 0 \\ \nabla \cdot (\rho \vec{u} \vec{u}) &= -\nabla p + \nabla \cdot (\mu \nabla \vec{u}) + \rho \vec{g}\end{aligned}\quad (4)$$

For simplicity, we used a fixed interface where Marangoni stresses are balanced by viscous stresses, consistently with previous work on interfaces with surfactants⁴³. The curvature-dependent Laplace pressure is also considered and applied to the droplet¹³,

$$\vec{t} \cdot \nabla_s \gamma = \delta(\vec{t} \cdot \Pi \cdot \vec{n}) \quad (5)$$

where Π is the stress tensor, \vec{n} is the unit outer normal vector, \vec{t} is the unit vector tangential to the interface and ∇_s is the gradient along the interface. The operator δ represents the difference across the interface. No slip boundary condition is applied to the walls in the computational domain except the droplet bottom where an inlet boundary condition is applied and the top wall where an outlet boundary condition is enforced.

Supporting Information

Supporting Information pdf

Supporting video 1

Supporting video 2

Supporting video 3

Supporting video 4

Acknowledgments

This work is supported by the startup fund provided by the University of California, Santa Barbara. S.S. and X.L. acknowledge funding support from NSF-CASIS Transport Phenomena grant No. 2025655 to Y.Z., P.L.F and J.R.A. Partial support from ARO MURI W911NF-17-1-0306 to P.L.F. is gratefully acknowledged.

References

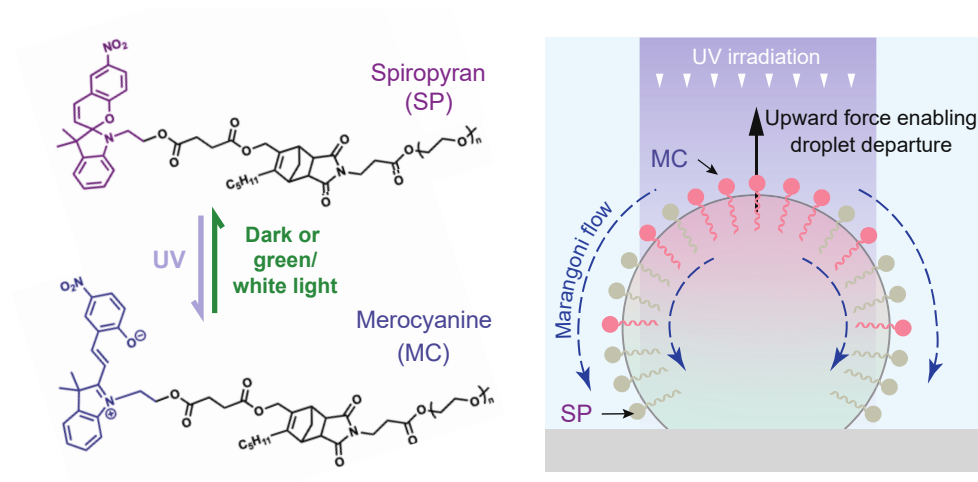
- (1) Cho, H. J.; Preston, D. J.; Zhu, Y.; Wang, E. N. Nanoengineered Materials for Liquid–Vapour Phase-Change Heat Transfer. *Nat. Rev. Mater.* **2016**, *2*, 16092. <https://doi.org/10.1038/natrevmats.2016.92>.
- (2) Kim, H.; Yang, S.; Rao, S. R.; Narayanan, S.; Kapustin, E. A.; Furukawa, H.; Umans, A. S.; Yaghi, O. M.; Wang, E. N. Water Harvesting from Air with Metal–Organic Frameworks Powered by Natural Sunlight. *Science* **2017**, eaam8743. <https://doi.org/10.1126/science.aam8743>.
- (3) Lu, Z.; Zhu, W.; Yu, X.; Zhang, H.; Li, Y.; Sun, X.; Wang, X.; Wang, H.; Wang, J.; Luo, J.; Lei, X.; Jiang, L. Ultrahigh Hydrogen Evolution Performance of Under-Water “Superaerophobic” MoS₂ Nanostructured Electrodes. *Advanced Materials* **2014**, *26* (17), 2683–2687. <https://doi.org/10.1002/adma.201304759>.
- (4) Cao, Z.; Zhou, J.; Wei, J.; Sun, D.; Yu, B. Experimental and Numerical Study on Bubble Dynamics and Heat Transfer during Nucleate Boiling of FC-72. *International Journal of Heat and Mass Transfer* **2019**, *139*, 822–831. <https://doi.org/10.1016/j.ijheatmasstransfer.2019.05.061>.
- (5) Jaikumar, A.; Rishi, A.; Gupta, A.; Kandlikar, S. G. Microscale Morphology Effects of Copper–Graphene Oxide Coatings on Pool Boiling Characteristics. *Journal of Heat Transfer* **2017**, *139* (11). <https://doi.org/10.1115/1.4036695>.
- (6) Zhao, Q.; Cui, H.; Wang, Y.; Du, X. Microfluidic Platforms toward Rational Material Fabrication for Biomedical Applications. *Small* **2020**, *16* (9), 1903798. <https://doi.org/10.1002/sml.201903798>.
- (7) Prashanth, S.; Subbaya, K.; Kundachira, N.; Sachhidananda, S. Fiber Reinforced Composites - A Review. *Journal of Material Sciences & Engineering* **2017**, *6* (3), 1–6. <https://doi.org/10.4172/2169-0022.1000341>.
- (8) Liu, Y.; Andrew, M.; Li, J.; Yeomans, J. M.; Wang, Z. Symmetry Breaking in Drop Bouncing on Curved Surfaces. *Nat Commun* **2015**, *6* (1), 10034. <https://doi.org/10.1038/ncomms10034>.
- (9) Feng, S.; Delannoy, J.; Malod, A.; Zheng, H.; Quéré, D.; Wang, Z. Tip-Induced Flipping of Droplets on Janus Pillars: From Local Reconfiguration to Global Transport. *Science Advances* **2020**, *6* (28), eabb4540. <https://doi.org/10.1126/sciadv.abb4540>.
- (10) Liu, Y.; Moevius, L.; Xu, X.; Qian, T.; Yeomans, J. M.; Wang, Z. Pancake Bouncing on Superhydrophobic Surfaces. *Nature Phys* **2014**, *10* (7), 515–519. <https://doi.org/10.1038/nphys2980>.

- (11) Tsai, P.; Pacheco, S.; Pirat, C.; Lefferts, L.; Lohse, D. Drop Impact upon Micro- and Nanostructured Superhydrophobic Surfaces. *Langmuir* **2009**, *25* (20), 12293–12298. <https://doi.org/10.1021/la900330q>.
- (12) Chen, L.; Liu, M.; Lin, L.; Zhang, T.; Ma, J.; Song, Y.; Jiang, L. Thermal-Responsive Hydrogel Surface: Tunable Wettability and Adhesion to Oil at the Water/Solid Interface. *Soft Matter* **2010**, *6* (12), 2708–2712. <https://doi.org/10.1039/C002543G>.
- (13) Maass, C. C.; Krüger, C.; Herminghaus, S.; Bahr, C. Swimming Droplets. *Annual Review of Condensed Matter Physics* **2016**, *7* (1), 171–193. <https://doi.org/10.1146/annurev-conmatphys-031115-011517>.
- (14) Miljkovic, N.; Preston, D. J.; Enright, R.; Wang, E. N. Electric-Field-Enhanced Condensation on Superhydrophobic Nanostructured Surfaces. *ACS Nano* **2013**, *7* (12), 11043–11054. <https://doi.org/10.1021/nn404707j>.
- (15) Wang, W.; Timonen, J. V. I.; Carlson, A.; Drotlef, D.-M.; Zhang, C. T.; Kolle, S.; Grinthal, A.; Wong, T.-S.; Hatton, B.; Kang, S. H.; Kennedy, S.; Chi, J.; Blough, R. T.; Sitti, M.; Mahadevan, L.; Aizenberg, J. Multifunctional Ferrofluid-Infused Surfaces with Reconfigurable Multiscale Topography. *Nature* **2018**, *559* (7712), 77–82. <https://doi.org/10.1038/s41586-018-0250-8>.
- (16) Choi, K.; Ng, A. H. C.; Fobel, R.; Wheeler, A. R. Digital Microfluidics. *Annual Review of Analytical Chemistry* **2012**, *5* (1), 413–440. <https://doi.org/10.1146/annurev-anchem-062011-143028>.
- (17) Hao, C.; Liu, Y.; Chen, X.; He, Y.; Li, Q.; Li, K. Y.; Wang, Z. Electrowetting on Liquid-Infused Film (EWOLF): Complete Reversibility and Controlled Droplet Oscillation Suppression for Fast Optical Imaging. *Sci Rep* **2014**, *4* (1), 6846. <https://doi.org/10.1038/srep06846>.
- (18) Zhu, Y.; Antao, D. S.; Xiao, R.; Wang, E. N. Real-Time Manipulation with Magnetically Tunable Structures. *Adv. Mater.* **2014**, *26* (37), 6442–6446. <https://doi.org/10.1002/adma.201401515>.
- (19) He, S.; Meng, Y.; Tian, Y. Correlation Between Adsorption/Desorption of Surfactant and Change in Friction of Stainless Steel in Aqueous Solutions Under Different Electrode Potentials. *Tribol Lett* **2011**, *41* (3), 485–494. <https://doi.org/10.1007/s11249-010-9604-6>.
- (20) Li, J.; Ha, N. S.; Liu, T. ‘Leo’; van Dam, R. M.; ‘CJ’ Kim, C.-J. Ionic-Surfactant-Mediated Electro-Dewetting for Digital Microfluidics. *Nature* **2019**, *572* (7770), 507–510. <https://doi.org/10.1038/s41586-019-1491-x>.
- (21) Cho, H. J.; Mizerak, J. P.; Wang, E. N. Turning Bubbles on and off during Boiling Using Charged Surfactants. *Nat Commun* **2015**, *6*, 8599. <https://doi.org/10.1038/ncomms9599>.
- (22) Lv, C.; Varanakkottu, S. N.; Baier, T.; Hardt, S. Controlling the Trajectories of Nano/Micro Particles Using Light-Actuated Marangoni Flow. *Nano Lett.* **2018**, *18* (11), 6924–6930. <https://doi.org/10.1021/acs.nanolett.8b02814>.
- (23) Xiao, Y.; Zarghami, S.; Wagner, K.; Wagner, P.; Gordon, K. C.; Florea, L.; Diamond, D.; Officer, D. L. Moving Droplets in 3D Using Light. *Advanced Materials* **2018**, *30* (35), 1801821. <https://doi.org/10.1002/adma.201801821>.
- (24) Diguet, A.; Guillermic, R.-M.; Magome, N.; Saint-Jalmes, A.; Chen, Y.; Yoshikawa, K.; Baigl, D. Photomanipulation of a Droplet by the Chromocapillary Effect. *Angewandte Chemie International Edition* **2009**, *48* (49), 9281–9284. <https://doi.org/10.1002/anie.200904868>.

- (25) Li, M.; Hosseinzadeh, M.; Pagonabarraga, I.; Seemann, R.; Brinkmann, M.; Fleury, J.-B. Kinetics of Active Water/Ethanol Janus Droplets. *Soft Matter* **2020**, *16* (29), 6803–6811. <https://doi.org/10.1039/D0SM00460J>.
- (26) Golestanian, R.; Liverpool, T. B.; Ajdari, A. Propulsion of a Molecular Machine by Asymmetric Distribution of Reaction Products. *Phys. Rev. Lett.* **2005**, *94* (22), 220801. <https://doi.org/10.1103/PhysRevLett.94.220801>.
- (27) Muller, J.; Wedershoven, H. M. J. M.; Darhuber, A. A. Monitoring Photochemical Reactions Using Marangoni Flows. *Langmuir* **2017**, *33* (15), 3647–3658. <https://doi.org/10.1021/acs.langmuir.7b00278>.
- (28) Grawitter, J.; Stark, H. Feedback Control of Photoresponsive Fluid Interfaces. *Soft Matter* **2018**, *14* (10), 1856–1869. <https://doi.org/10.1039/C7SM02101A>.
- (29) Seshadri, S.; Bailey, S. J.; Zhao, L.; Fisher, J.; Sroda, M.; Chiu, M.; Stricker, F.; Valentine, M. T.; Read de Alaniz, J.; Helgeson, M. E. Influence of Polarity Change and Photophysical Effects on Photosurfactant-Driven Wetting. *Langmuir* **2021**, *37* (33), 9939–9951. <https://doi.org/10.1021/acs.langmuir.1c00769>.
- (30) Setaro, A.; Bluemmel, P.; Maity, C.; Hecht, S.; Reich, S. Non-Covalent Functionalization of Individual Nanotubes with Spiropyran-Based Molecular Switches. *Advanced Functional Materials* **2012**, *22* (11), 2425–2431. <https://doi.org/10.1002/adfm.201102451>.
- (31) Klajn, R. Spiropyran-Based Dynamic Materials. *Chem. Soc. Rev.* **2013**, *43* (1), 148–184. <https://doi.org/10.1039/C3CS60181A>.
- (32) Kathan, M.; Hecht, S. Photoswitchable Molecules as Key Ingredients to Drive Systems Away from the Global Thermodynamic Minimum. *Chem Soc Rev* **2017**, *46* (18), 5536–5550. <https://doi.org/10.1039/c7cs00112f>.
- (33) Bailey, S. J.; Discekici, E. H.; Barbon, S. M.; Nguyen, S. N.; Hawker, C. J.; Read de Alaniz, J. Norbornadiene Chain-End Functional Polymers as Stable, Readily Available Precursors to Cyclopentadiene Derivatives. *Macromolecules* **2020**, *53* (12), 4917–4924. <https://doi.org/10.1021/acs.macromol.0c00967>.
- (34) St. Amant, A. H.; Discekici, E. H.; Bailey, S. J.; Zayas, M. S.; Song, J.-A.; Shankel, S. L.; Nguyen, S. N.; Bates, M. W.; Anastasaki, A.; Hawker, C. J.; Read de Alaniz, J. Norbornadienes: Robust and Scalable Building Blocks for Cascade “Click” Coupling of High Molecular Weight Polymers. *J. Am. Chem. Soc.* **2019**, *141* (34), 13619–13624. <https://doi.org/10.1021/jacs.9b06328>.
- (35) Stauffer, C. E. The Measurement of Surface Tension by the Pendant Drop Technique. *J. Phys. Chem.* **1965**, *69* (6), 1933–1938. <https://doi.org/10.1021/j100890a024>.
- (36) Chang, C.-H.; Franses, E. I. Adsorption Dynamics of Surfactants at the Air/Water Interface: A Critical Review of Mathematical Models, Data, and Mechanisms. *Colloids and Surfaces A: Physicochemical and Engineering Aspects* **1995**, *100*, 1–45. [https://doi.org/10.1016/0927-7757\(94\)03061-4](https://doi.org/10.1016/0927-7757(94)03061-4).
- (37) Saien, J.; Akbari, S. Interfacial Tension of Toluene + Water + Sodium Dodecyl Sulfate from (20 to 50) °C and PH between 4 and 9. *J. Chem. Eng. Data* **2006**, *51* (5), 1832–1835. <https://doi.org/10.1021/je060204g>.
- (38) Zhang, Q.; Pang, Y.; Schiffbauer, J.; Jemcov, A.; Chang, H.-C.; Lee, E.; Luo, T. Light-Guided Surface Plasmonic Bubble Movement via Contact Line De-Pinning by In-Situ Deposited Plasmonic Nanoparticle Heating. *ACS Appl. Mater. Interfaces* **2019**, *11* (51), 48525–48532. <https://doi.org/10.1021/acsami.9b16067>.

- (39) Yang, Z.; Wei, J.; Sobolev, Y. I.; Grzybowski, B. A. Systems of Mechanized and Reactive Droplets Powered by Multi-Responsive Surfactants. *Nature* **2018**, *553* (7688), 313–318. <https://doi.org/10.1038/nature25137>.
- (40) Hanif, N. M.; Adnan, S. N. N.; Latif, M. T.; Zakaria, Z.; Abdullahand, P.; Othman, M. R. The Composition of Surfactants in River Water and Its Influence to the Amount of Surfactants in Drinking Water. *World Applied Sciences Journal* **2012**, *17* (8), 970–975.
- (41) Kabir, E.; Kumar, P.; Kumar, S.; Adelodun, A. A.; Kim, K.-H. Solar Energy: Potential and Future Prospects. *Renewable and Sustainable Energy Reviews* **2018**, *82*, 894–900. <https://doi.org/10.1016/j.rser.2017.09.094>.
- (42) Raymo, F. M.; Giordani, S. Signal Processing at the Molecular Level. *J. Am. Chem. Soc.* **2001**, *123* (19), 4651–4652. <https://doi.org/10.1021/ja005699n>.
- (43) Peaudecerf, F. J.; Landel, J. R.; Goldstein, R. E.; Luzzatto-Fegiz, P. Traces of Surfactants Can Severely Limit the Drag Reduction of Superhydrophobic Surfaces. *PNAS* **2017**, *114* (28), 7254–7259. <https://doi.org/10.1073/pnas.1702469114>.

TOC graphic



Synopsis:

We demonstrate a new mechanism to drive bubble and droplet departure from substrates, using only targeted light and a low concentration of light-sensitive surfactant.